ASM Handbook, Volume 22A: Fundamentals of Modeling for Metals Processing
D.U. Furrer and S.L. Semiatin, editors, p 362-374

Modeling of Hot Tearing and Other Defects in Casting Processes

Brian G. Thomas, University of Illinois (UIUC)

AS COMPUTATIONAL MODELS MATURE, their practical benefit to improving casting processes is growing. Accurate calculation of fluid velocities, temperature, microstructure, and stress evolution is just the first step. Achieving tangible improvements to casting processes requires the accurate prediction of actual casting defects and product properties. Defects that form during solidification are important not only to the casting engineer but also to engineers involved in subsequent manufacturing processes and evaluation. Solidification defects are responsible for many of the defects in final manufactured products and failures in service. They originate from inclusion entrapment, segregation, shrinkage cavities, porosity, mold-wall interactions, cracks, and many other sources that are process-specific. Casting defects can be modeled by extending the results of casting simulations through postprocessing and/or by solving further coupled equations that govern these phenomena. The prediction of defect formation is made difficult by the staggering complexity of the phenomena that arise during commercial casting processes. This article introduces some of the concepts involved in modeling some of these solidification defects and focuses in more detail on hot tearing.

Inclusions

Inclusions are responsible for many serious surface defects and internal quality problems in cast products. They arise from foreign particles, such as eroded sand particles, and impurities remaining in the liquid metal after upstream refining (Ref 1). Nonmetallic inclusion particles act as sites of stress concentration and hydrogen gas nucleation, leading to lower fatigue life, hydrogen embrittlement, surface defects, and other problems in the final product. Predicting their damage requires knowledge of the number, size distribution, composition, and morphology of the inclusions coming from upstream processing prior to casting. Obtaining this knowledge ideally involves modeling the multiphase fluid flow, turbulent mixing and diffusion, species transport, chemical reactions, and particle interactions that create the inclusions in upstream processes.

Considerable modeling of these phenomena has been addressed in previous simulations of vacuum degassers, R-H degassers (a type of recirculating degasser), ladles, tundishes, and other refining vessels and transfer operations used in metallurgical processing (Ref 2). These models solve the multiphase Navier-Stokes equations for turbulent fluid flow, using software such as FLUENT (Ref 3), and provide the flow field for subsequent simulation of inclusion particle transport. The first challenge is to properly incorporate the phenomena that drive the flow, which usually include the buoyancy of injected gas bubbles (Ref 4), which depends on the shape of the bubbles, ranging from spherical caps to spheres. Other effects important to accurately computing the flow field may include natural convection, which requires a coupled heat-transport solution for the temperature field. When electromagnetic stirring is used, these forces require modeling the applied magnetic field. Another challenge is to incorporate the effects of turbulence. Computationally-efficient choices include simple "mixing-length" models, the two-equation models such as k-ε to simulate the time-average flow pattern. Large-eddy simulation (LES) models can simulate the details of the time-evolving turbulent vortices, but at great computational expense. These methods have been compared with each other and with measurements of fluid flow in continuous casting (Ref 5–7).

Formation. Modeling the thermodynamics and kinetics of particle formation, transport, collisions, and removal or entrapment in the molten metal during upstream refining processes is the next crucial step. Thermodynamic reactions to quantify the precipitates that form in these multicomponent alloy systems can be predicted by simultaneous solution of chemical equilibrium equations, where the biggest challenge is to find accurate activity coefficients. Equilibrium compositions can also be found by comparing free-energy functions, such as used in Thermo-Calc (Ref 8), FACT-Sage (Ref 9), MTDATA (Ref 10), Gemini (Ref 11), and other thermodynamic modeling software. The kinetics of nonmetallic inclusion formation are generally controlled by species transport in the liquid and at reaction interfaces, such as the slag-metal surface, where droplets of the different liquid phases, solid particles, and gas bubbles interact. The physical entrainment of slag particles into the molten metal is another important source of inclusions (Ref 12), which requires transient multiphase modeling of the free surface, considering its breakup into droplets and surface tension effects, and pushes current modeling capabilities to their limit.

Another important source of inclusions is reoxidation of the molten metal by exposure to air. Oxygen absorbs rapidly from the atmosphere into any exposed molten metal and combines to form precipitates, which has been predicted in molten steel from the alloy content (Ref 13). Predictions are limited by understanding of the entrainment of oxygen from the atmosphere, the turbulent flow of the liquid steel during pouring, which determines the gas-metal interface shape, and the internal transport and reactions of chemical species in the molten metal.

Transport. The transport of particles through the flowing metal is the next crucial step to determine the inclusion distribution in the final product and can be modeled in several ways (Ref 14). Although the effect of bubbles on the flow pattern can be modeled effectively using Eulerian-Eulerian multiphase models, the fate of inclusion distributions is best modeled via Lagrangian particle tracking. In this method, the trajectories of many particles are integrated from the local velocity field, based on previous solution of the fluid velocities of a mold-filling simulation. The effect of turbulence on the chaotic particle paths is very important and is best

modeled with the transient turbulent velocity field, using LES (Ref 15). In more computationally-efficient time-averaged simulations of the turbulent flow field, the effect of turbulence on particle motion can be approximated using methods such as "random walk," where the velocity at each time increment is given a randomly-generated component with magnitude proportional to the local turbulence level (Ref 3). This method has been applied successfully to simulate particle motion in continuous casting molds (Ref 16).

Inclusion particle size distributions evolve during transport due to collisions with each other and by their attachment to the surface of bubbles. Collisions can be modeled by tracking the evolution in the number distribution of particles in each size range, including the local effects of Brownian motion, turbulence, and diffusion, which is aided by size-grouping models to cover the large range of particle sizes (Ref 17). Attachment and removal by bubbles can be modeled by computing the attachment rates of different particle sizes to different bubble sizes and shapes in computational models of these microscale phenomena (Ref 16, 18). These attachment rates can then be incorporated into the macroscale models of fluid and particle trajectories (Ref 16, 18). In the extreme, inclusions may agglomerate into large clogs, which can restrict the flow of molten metal, cause detrimental changes in the downstream flow pattern, and can lead to catastrophic defects in the final product. Modeling and analysis of clogging is a complex subject that has been reviewed elsewhere (Ref 19).

Capture. Particle capture into the solidification front is a critical step during the modeling of inclusion transport. Small particles flow between the dendrites, so they can be modeled as entrapped when they touch a domain wall. Larger particles may be pushed by the interface or engulfed by a fast-moving planar front (Ref 20). More often, they are entrapped when they are suspended in front of the solidification front long enough for the dendrites to surround them. Entrapment is greatly lessened by tangential flow across the solidification front (Ref 21). A criterion for entrapment has been developed based on balancing the many forces that act on a particle suspended at the interface (Ref 21). Particles that never touch the interface, or escape capture, eventually may be removed if the flow pattern transports them to the casting boundaries, such as the top surface of some processes, where they can enter the slag layer.

The final step is to predict the property changes caused by the entrapped inclusions, which is a challenging modeling task and depends on downstream processing, such as rolling and heat treatment. Even with simply cooling to ambient, precipitation continues in the solid state, where the inclusion distribution is greatly affected by kinetic delays due to nucleation and solid-state diffusion (Ref 22). This is further complicated by preferential precipitation at grain boundaries and compatible existing inclusions and is affected by strains, local microsegregation, and many other phenomena. Clearly, the modeling of inclusions is a challenging task.

Segregation

Segregation is caused by the partitioning of alloying elements between the liquid and solid phases during solidification. Because species diffusion in the solid is very slow, this phenomenon is usually manifested by small-scale composition differences, called microsegregation, which explains how the spaces between dendrites are enriched in alloy relative to the dendrite centers. Although it contributes greatly to macrosegregation, porosity, inclusions, and other defects, microsegregation alone is not usually considered a defect, and it can be removed by homogenization heat treatment. When fluid flow is present, however, large-scale species transport leads to macrosegregation, where the composition differences arise over large distances, such as between the center and surface of a casting. This serious defect cannot be removed. It is extremely difficult to predict, because it involves so many different coupled phenomena, and at vastly different length and time scales. In addition to predicting fluid flow, species transport, and solidification, segregation requires prediction of the dendrite morphology and microstructure and the complete stress state, including deformation of the spongy mushy zone (Ref 23) and mechanical bulging and bending of the casting surface (Ref 24). Moreover, the fluid flow must be accurately characterized at both the microscopic scale between dendrite arms and at the macroscopic scale of the entire casting. Each of these modeling tasks is a large discipline that has received significant effort over several decades.

Segregation is the main phenomenon responsible for many different kinds of special defects that only affect particular casting processes. For example, "freckle" defects can arise during the directional solidification of turbine blades when buoyancy-driven flow allows winding vertical channels to penetrate between dendrites and become filled with segregated liquid near the end of solidification (Ref 25). Inverse segregation or surface exudation in direct-chill continuous casting of aluminum ingots arises during the initial stages of solidification when thermal stress pushes out droplets of enriched interdendritic liquid through pores in the spongy mushy zone where it extends to the ingot surface (Ref 26). A comprehensive summary of the modeling of this important class of defects is beyond the scope of this article, and reviews of various aspects of this complex subject can be found elsewhere (Ref 23, 27–29).

Shrinkage Cavities, Gas Porosity, and Casting Shape

Shrinkage cavities are voids in a casting that form due to the thermal contraction of liquid pockets after they become surrounded by solid that prevents the feeding of additional liquid. Porosity is the name for small voids that form due to the evolution and entrapment of gas bubbles. These two important classes of defects are related. Both involve the entrapment of liquid pockets, a criterion for the nucleation of gas bubbles, and depend on the overall shrinkage of the casting, which requires a complete thermomechanical stress calculation, in addition to accurate prediction of fluid flow and solidification. A rough estimate of shrinkage cavity potential is possible from postprocessing analysis of the results of a simple solidification heat-transfer analysis, looking for regions where solid surrounds the liquid. This simple analysis can be automated by tracking parameters that represent shrinkage potential, such as the Niyama criterion (Ref 30, 31) More accurate prediction of shrinkage requires complete modeling of fluid flow, heat transfer, and thermal-stress analysis. The fluid flow analysis is further complicated by the need for accurate characterization of the permeability of the porous dendritic network, which also depends on the microstructure and alloy segregation. The stress analysis depends on the evolving strength of the solid, in addition to the mushy zone, interaction with the mold, and other phenomena that are discussed further in the section on hot tearing.

In addition to the phenomena that govern shrinkage cavity formation, gas porosity prediction also requires modeling the transport of dissolved gases, the nucleation of bubbles or gas pockets, and their possible transport after they form. This modeling also involves the same complications discussed in the prediction of inclusions, including nonequilibrium thermodynamics, chemical reactions, nucleation, precipitate formation, and growth kinetics. Indeed, precipitation reactions are alternative ways for the dissolved gases to be consumed. Finally, gas bubbles that float during solidification can collide and coalesce, depending on surface tension. When combined with improper venting, this can lead to the creation of a defect found at the top of foundry castings, known as a surface blow hole.

Shrinkage and porosity defects are related to the final shape of the casting. When the solid metal shell is strong enough to resist shrinkage and retain its external dimensions, internal shrinkage and porosity may be more problematic. In contrast, practices that lessen shrinkage and porosity may involve more external shrinkage of the exterior. Inaccurate final dimensions is another casting defect. Because comprehensive modeling of these defects requires the simultaneous solution of so many different

equation systems, with so many uncertain fundamental properties, this class of defects is difficult to predict and is the subject of intense ongoing research. The art of modeling these defects involves how to make simplifying assumptions with the least loss of accuracy. Further details on the current state of the art in modeling of this important class of defects is given elsewhere (Ref 28, 32, 33).

Mold-Wall Erosion

Feeding molten metal into the casting cavity is a critical operation where defects may arise. Excessive turbulence and velocity impingement of the molten metal can erode the surface of the mold wall, especially near the in-gate. In sand molds, this can dislodge sand particles to act as another source of inclusions in the final casting. Even with permanent metal molds such as used in pressure die casting, excessive velocity against the metal walls can locally erode the metal, enlarging the casting cavity and creating surface defects.

Erosion rate has been related to the metal velocity and other parameters in a few previous studies, based mainly on empirical correlations (Ref 34). For example, in die casting, erosion strength has been characterized by integrating the instantaneous velocity over the time of the injection cycle for each local portion of the mold-wall surface (Ref 35). The resulting contours over the mold surface can be correlated with erosion damage.

Erosion of the mold wall due to fluid flow also may remove protective surface coatings and allow chemical reactions between the mold and the exposed mold metal. Thus, the mechanical erosion may be accompanied by chemical erosion and/or metallurgical corrosion, which often act together to wear away the mold surface. Analysis of the chemical component requires consideration of the thermodynamic reactions and their kinetics. The interdiffusion of elements in the molten metal to contaminate the mold walls can lower the local melting temperature. This is responsible for the problem of soldering in aluminum die casting in steel molds (Ref 36, 37).

Mold-Wall Cracks

Cracks in the mold wall are another source of defects in the casting, in addition to lowering the lifetime of permanent molds. Mold cracks decrease the local heat-transfer rate, allowing local strain concentration in the adjacent solidifying metal and causing hot-tear cracks at the casting surface that mirror those in the mold. In water-cooled molds, mold cracks also pose a safety hazard, from the chance of molten metal contacting the cooling water. Mold cracks, or heat checks, are caused by repeated rapid and severe fluctuations in the mold surface temperature. They can be predicted from the results of a transient thermal-stress analysis of the mold itself, by combining the calculated inelastic strain (due to plasticity and creep) with measurements of cycles to failure from thermal-fatigue experiments. For example, surface cracks in copper molds used from continuous casting were predicted by comparing the results of transient three-dimensional finite-element analysis of the copper mold and its support structure during cyclic loading with measured fatigue cycle-to-failure data (Ref 38). In addition to adopting practices to lower the maximum surface temperature, the mold lifetime was predicted to increase by lessening constraint of the mold by loosening bolts (Ref 38, 39). Often, the prediction of mold cracks requires consideration of the chemical interaction of the liquid metal with the mold, such as formation of brass in copper molds by the preferential absorption of zinc from the molten metal.

Other Defects

Many other casting defects arise due to problems specific to individual processes. Grain defects, such as unwanted grain boundaries, are important in directional solidification processes, such as the casting of single-crystal turbine blades, where high-temporature creep resistance is the most important property. In the Czochralski process, where single crystals are slowly pulled from doped melts to cast rods for making semiconductor wafers, even dislocations are serious defects that must be minimized. Examples in foundry sand casting include cold shut, blow holes, liquid metal penetration into the sand grains, and other surface defects. Some insight into these defects can be found from the results of a solidification heat-transfer analysis. For example, problems related to cold shut can be estimated from a simulation if the molten metal freezes before the casting cavity is completely filled, leaving voids or seams at the junction where two streams met. Crystal defects depend on the temperature gradient across the solidification front. Further insight can be gained from direct modeling of the microstructure (Ref 40) and molecular dynamics or quantum-mechanics models of dislocations and other phenomena at the atomic scale (Ref 41). Many important process-specific defects have received little attention by the modeling community.

A final category of defects may be termed "goofups" because their cause is so obvious, and the solution involves, at most, only basic calculations. For example, a short pour occurs when the volume of metal poured is less than the volume of the casting cavity. Unsightly mismatch seams arise when the two halves of the foundry casting mold are not aligned due to poor maintenance of the hinges and pins. Although obvious, avoiding such defects requires careful and diligent operations. Here, expert-system-type software may help, aided in these examples by embedding simple volume calculations and tracking of maintenance schedules. The rest of this article focuses on the important defect of hot-tear crack formation.

Hot-Tear Cracks

Crack formation is caused by a combination of tensile stress and metallurgical embrittlement. Although solidifying metal is subject to embrittlement due to a number of different mechanisms at different temperature ranges, hot-tear cracks form near the solidus temperature. Embrittlement is so severe near this temperature that hot-tear cracks form at strains on the order of only 1%, making them responsible for most of the cracks observed in cast products. Hot-tear cracks form because thin liquid films between the dendrites at grain boundaries are susceptible to strain concentration, causing separation of the dendrites and intergranular cracks. The prediction of these cracks presents a formidable challenge to modellers, owing to the many complex, interacting phenomena that govern stress and embrittlement, some of which are not yet fully understood:

- Predicting temperature, strain, and stress during solidification requires calculation of the history of the cast product and its environment over huge temperature intervals. Characterizing the heat-transfer coefficients at the boundaries and interfaces is one of many difficulties.
- The mechanical problem is highly nonlinear, involving liquid-solid interaction and complex constitutive equations. Stress arises primarily from the mismatch of strains caused by large temperature gradients and depends on the time- and microstructure-dependent inelastic flow of the material. Even identifying the numerous metallurgical parameters involved in these relationships is a daunting task.
- The coupling between the thermal and the mechanical problems is an additional difficulty. This coupling comes from the mechanical interaction between the casting and the mold components, through gap formation or the buildup of contact pressure, locally modifying the heat exchange.
- Accounting for the mold and its interaction with the casting makes the problem multidomain, usually involving numerous deformable components with coupled interactions and contact analysis.
- Cast parts usually have very complex three-dimensional shapes, which puts great demands on the interface between computer-aided design and the mechanical solvers and on computational resources.
- The main cause of embrittlement is the segregation of solute impurities and alloying elements to the interdendritic liquid between primary grains, which lowers the solidus temperature locally. Segregation is most severe, and thus most important, at the grain boundaries, owing to the greater local

interdenritic spacing locally, which allows the liquid to persist longer between grain boundaries.

- Larger primary grain size increases strain concentration and embrittlement, so it must also be predicted. Because the grain size evolves with time, the grain size in the final cooled microstructure differs from the primary grain size, so grain size measurements for model validation should be inferred from analysis of the microsegregation pattern.
- Stress on the liquid films depends on the ability of liquid to flow through the dendritic structure to feed the volumetric shrinkage, relative to the strength of the surrounding dendritic skeleton. Thus, accurate permeability models are required for the mushy zone, which, in turn, require accurate prediction of the microstructure, including the dendrite arm shapes, especially at the grain boundaries.
- Crack prediction requires modeling the distribution of supersaturated dissolved gas and its nucleation into pores or crack surfaces.
- The formation of solid precipitates tends to pin the primary grain boundaries, enhancing strain concentration. The interfering precipitates also act as nucleation sites for both gas bubbles and voids, both of which increase embrittlement. Modeling precipitation is difficult, owing to the multicomponent nature of commercial alloys and the importance of kinetic delays.
- The subsequent refilling of hot tears with segregated liquid alloy can cause internal defects that are just as serious as exposed surface cracks, which oxidize. This again requires accurate prediction of both interdendritic and intergranular solute flow.
- The most important parameters to hot tearing— the stress-tensor field, which acts to concentrate tensile strain in liquid regions of the mushy zone, and the fluid-velocity vector field, which acts to fill the voids— are both three-dimensional time-varying quantities that depend greatly on the orientation and shape of the microstructure. Thus, even empirical criteria to predict hot tears depend on conducting experiments with the proper load orientation, rates, and microstructures.
- The important length scales range from micrometers (dendrite arm shapes) to tens of meters (metallurgical length of a continuous caster), with a similar huge order-of-magnitude range in time scales.

Heat-Transfer Modeling

Accurate calculation of the evolving temperature distribution during the casting process is the first and most important step in the analysis of hot tears. In addition to solving the transient heat-transport equation with phase change, this critical task usually requires coupling with turbulent fluid flow during mold filling and interaction with the mold walls, with particular attention to the interfacial gap.

Heat transfer across the mold-casting interface depends on the size of the gap (if open) or the contact pressure (if closed), so coupling with results from a mechanical analysis is often needed. Figure 1 shows the changes in interfacial heat transfer for these two cases. When a gap opens between the casting and the mold due to their relative deformation, the heat transfer drops in proportion to the size of the gap. Heat flows across the interface, q_{gap}, by conduction through the gas within the gap and by radiation between the two parallel surfaces:

$$q_{gap} = \frac{k_{gas}}{g}(T_c - T_m) + \frac{\sigma(T_c^4 - T_m^4)}{\frac{1}{\varepsilon_c} + \frac{1}{\varepsilon_m} - 1} \qquad \text{(Eq 1)}$$

where k_{gas} (T) is the thermal conductivity of the gap; g is the gap thickness; T_c and T_m are the local surface temperature of the casting and mold, respectively; ε_c and ε_m are emissivities; and σ is the Stefan-Boltzmann constant. To avoid numerical problems at small gap sizes, this function should be truncated to a finite value, h_0, which corresponds to the closed-gap case and depends on the average roughness. More sophisticated functions can be applied to account for mold coating layers, different material layers, radiation conduction, contact resistances to incorporate surface roughness, and other phenomena. Specific examples of these gap heat-transfer laws are provided elsewhere for continuous casting with oil lubrication (Ref 42) and mold flux (Ref 43).

When contact between the mold and casting is good, the interfacial heat flux increases with contact pressure according to a power law (Ref 44), such as:

$$q_{contact} = (h_0 + Ap_c^B)(T_c - T_m) \qquad \text{(Eq 2)}$$

where p_c is the contact pressure, and A and B are fitting parameters that depend on the materials, lubricants, roughnesses, and temperature. After removal from the mold, heat transfer is given by uncoupled surface convection coefficients. Accurate characterization of the surface heat flux for all of these conditions requires careful calibration and validation with experimental measurements and is a critical step in modeling.

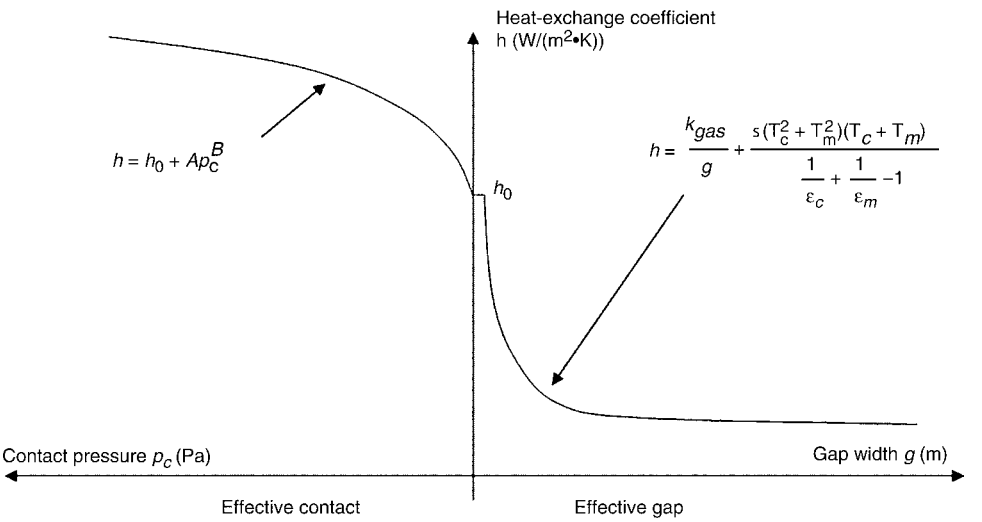

Fig. 1 Modeling heat-transfer coefficient across the mold-casting gap

Thermomechanical Modeling

Prediction of the displacements, strains, and stresses during the casting process is the next step in predicting residual stress, the distorted shape, and crack defects, including hot tears. As previously mentioned, stress analysis is also important in the prediction of porosity and segregation. The modeling of mechanical behavior requires solution of the equilibrium or momentum equations relating force and stress, the compatibility equations relating strain and displacement, and the constitutive equations relating stress and strain. This is because the boundary conditions specify either force or displacement at different regions of the domain boundaries.

Governing Equations. The conservation of force (steady-state equilibrium) or momentum (transient conditions) can be expressed by:

$$\rho\left(\frac{\partial \boldsymbol{v}}{\partial t} + \boldsymbol{v} \cdot \nabla \boldsymbol{v}\right) = \nabla \cdot \boldsymbol{\sigma} + \rho \mathbf{g} \qquad \text{(Eq 3)}$$

where $\boldsymbol{\sigma}$ is the stress tensor, ρ is the density, $\mathbf{g}$ is the gravitational acceleration, $\mathbf{v}$ is the velocity field, ∇ is the gradient operator and matrices (vectors and tensors) are denoted in bold. Once solidified, the velocity terms that comprise the left side of Eq 3 can be neglected.

The strains that dominate thermomechanical behavior during solidification are on the order of only a few percent, prior to crack formation. With small gradients of spatial displacement,

$\nabla \mathbf{u} = \partial \mathbf{u}/\partial \mathbf{x}$, the compatibility equations simplify to (Ref 45):

$$\boldsymbol{\varepsilon} = \frac{1}{2}\left(\nabla \mathbf{u} + (\nabla \mathbf{u})^{\mathrm{T}}\right) \quad \text{(Eq 4)}$$

where $\boldsymbol{\varepsilon}$ is the strain tensor, $\mathbf{u}$ is the displacement vector, and $^{\mathrm{T}}$ denotes transpose. This small-strain assumption simplifies the analysis considerably. The compatibility equations can also be expressed as a rate formulation, where strains become strain rates and displacements become velocities. This formulation is more convenient for a transient computation with time integration involving fluid flow and/or large deformation.

Choosing constitutive models to relate stress and strain is a very challenging aspect of stress analysis of solidification, because it depends on accurately capturing the highly nonlinear evolution of the material microstructure with numerical parameters. Traditionally, this is accomplished with a family of elastic-plastic stress-strain curves at the appropriate temperatures and strain rate(s) and perhaps by adding a separate strain-rate function of temperature, stress, and time to account for the time-dependent softening effects of creep.

However, the state variables of strain and time are not enough to quantify the strength of the material, especially during loading reversals. Furthermore, the effects of plastic strain and creep-strain rate are not independent. Thus, unified models have been developed that combine the different microstructural mechanisms together in terms of state variables that relate more closely to fundamental microstructural parameters such as dislocation density. Many models of different complexity can be found in the literature (Ref 46, 47). In their simplest form, these constitutive equations for metals are often expressed in terms of the state variables of temperature and inelastic strain:

$$\dot{\boldsymbol{\varepsilon}} = \dot{\boldsymbol{\varepsilon}}^{\mathrm{el}} + \dot{\boldsymbol{\varepsilon}}^{\mathrm{in}} + \dot{\boldsymbol{\varepsilon}}^{\mathrm{th}} \quad \text{(Eq 5)}$$

$$\dot{\boldsymbol{\varepsilon}}^{\mathrm{el}} = \frac{1+\nu}{E}\dot{\boldsymbol{\sigma}} - \frac{\nu}{E}\mathrm{tr}(\dot{\boldsymbol{\sigma}})\mathbf{I} + \dot{T}\frac{\partial}{\partial T}\left(\frac{1+\nu}{E}\right)\boldsymbol{\sigma} - \dot{T}\frac{\partial}{\partial T}\left(\frac{\nu}{E}\right)\mathrm{tr}(\boldsymbol{\sigma})\mathbf{I} \quad \text{(Eq 6)}$$

$$\dot{\boldsymbol{\varepsilon}}^{\mathrm{in}} = f(\sigma, T, \text{structure}) \quad \text{(Eq 7)}$$

$$\dot{\boldsymbol{\varepsilon}}^{\mathrm{th}} = \left[\sqrt[3]{\frac{\rho(T_0)}{\rho}} - 1\right]\mathbf{I} \quad \text{(Eq 8)}$$

These tensor equations are expressed in terms of rates, where an overdot is the time derivative, tr is the trace of a matrix, $\mathbf{I}$ is the identity tensor, and every variable should depend on temperature, T. The strain-rate tensor, $\dot{\boldsymbol{\varepsilon}}$, is split into an elastic component $\left(\dot{\boldsymbol{\varepsilon}}^{\mathrm{el}}\right)$, an inelastic (nonreversible) component $\left(\dot{\boldsymbol{\varepsilon}}^{\mathrm{in}}\right)$, and a thermal component $\left(\dot{\boldsymbol{\varepsilon}}^{\mathrm{th}}\right)$. Equation 6 is the hypoelastic Hooke's law, where E is Young's modulus, v is the Poisson's coefficient, and $\dot{\boldsymbol{\sigma}}$ is the time derivative of the stress tensor $\boldsymbol{\sigma}$. Equation 7 gives a framework for evolving the inelastic strain tensor, $\boldsymbol{\varepsilon}^{\mathrm{in}}$, which is often used as the only parameter to characterize material structure. The thermal strains (Eq 8) include the solidification shrinkage and are based on the temperature field solved with the heat-transfer model. Care should be taken in choosing a consistent reference temperature, T_0, and in differentiating to extract the thermal strain rate, which can be accomplished numerically. Finding suitable constitutive equations to characterize the material mechanical response for the wide range of conditions experienced during solidification is a formidable task that requires careful experiments under different loading conditions, a reasonable form for the theoretical model, and advanced fitting procedures to extract the model coefficients.

Solution Strategies. Thermomechanical analysis of casting processes poses special difficulties due to the simultaneous presence of liquid, mushy, and solid regions that move with time as solidification progresses, the highly nonlinear constitutive equations, complex three-dimensional geometries, coupling with the thermal analysis, interaction with the mold, and many other reasons. Several different strategies have been developed, according to the process and model objectives:

- A first strategy is to perform a small-strain thermomechanical analysis on just the solidified portion of the casting domain, extracted from the thermal analysis results. This strategy is convenient when the solidification front is stationary, such as the continuous casting of aluminum (Ref 48) and steel (Ref 42, 49). For transient problems, such as the prediction of residual stress and shape (butt-curl) during startup of the direct-chill and electromagnetic continuous casting processes for aluminum ingots, the domain can be extended in time by adding layers (Ref 48).
- A second popular strategy considers the entire casting as a continuum, modifying the parameters in the constitutive equations for the liquid, mushy, and solid regions according to the temperature and phase fraction. For example, liquid can be treated by setting the strains to zero when the temperature is above the solidus temperature. The primary unknowns are the displacements or displacement increments. To facilitate the tracking of state variables, a Lagrangian formulation is adopted, where the domain follows the material. This popular approach can be used with structural finite-element codes, such as MARC (Ref 50) or ABAQUS (Ref 51), and with commercial solidification codes or special-purpose software, such as ALSIM (Ref 52)/ALSPEN (Ref 53), CASTS (Ref 54), CON2D (Ref 55, 56), Magmasoft (Ref 57), and Procast (Ref 58, 59). It has been applied successfully to simulate deformation and residual stress in shape castings (Ref 60, 61), direct chill casting of aluminum (Ref 48, 52, 53, 60, 62, 63), and continuous casting of steel (Ref 55, 64). Time integration of the highly nonlinear constitutive equations can benefit from special local-global integration numerical methods (Ref 56) or recent explicit methods (Ref 65). Assuming small strain and avoiding Poisson's ratio close to 0.5 for stability reasons (Ref 66, 67) means that the liquid phase is not modeled accurately. Thus, some phenomena must be incorporated from other models, such as heat transfer from impinging liquid jets (Ref 68) and fluid feeding into the mushy zone (Ref 55).
- A third strategy simulates the entire casting, treating the mass and momentum equations of the liquid and mushy regions with a mixed velocity-pressure formulation. The primary unknowns are the velocity (time derivative of displacement) and pressure fields, which makes it easier to impose the incompressibility constraints and to handle hydrostatic pressure loading. Indeed, the velocity-pressure formulation is also applied to the equilibrium of the solid regions, in order to provide a single continuum framework for the global numerical solution. This strategy has been implemented into codes dedicated to casting analysis, such as THERCAST (Ref 64, 69, 70) and VULCAN (Ref 71). If stress prediction is not important so that elastic strains can be ignored, then this formulation simplifies to a standard fluid-flow analysis, which is useful in the prediction of bulging and shape in large-strain processes. For problems involving large strain, such as squeeze casting, this strategy is suited to an arbitrary Lagrangian Eulerian (ALE) formulation. In a Eulerian formulation, material moves through the computational grid, which remains stationary in the laboratory frame of reference and requires careful updating of the state variables. In ALE, mesh updating is partially independent of the material velocity to maintain the quality of the computational grid. Further details are provided elsewhere (Ref 69, 72).

Hot-Tearing Criteria

The next step is to quantify embrittlement and to incorporate it with the thermal-stress analysis to predict hot-tear cracks. Hot-tearing phenomena are too complex, too small-scale, and insufficiently understood to model in detail as part of the macroscale thermomechanical analysis. Thus, several different criteria and approaches have been developed to predict hot tears from the results of such analyses. This topic is the focus of many ongoing research efforts, and although many of these criteria

reproduce observed trends, much more work is needed before quantitative predictions are reliable.

Different approaches are needed for different microstructures and metals, according to the most important phenomena that govern crack formation. Hot-tear cracks forming within large networks of mushy, equiaxed grains require accurate constitutive models to quantify the rheology of the mushy region. Cracks between columnar grains require models that incorporate the balance between liquid feeding between dendrites and tensile deformation perpendicular to the direction of dendrite growth. The hot tearing of aluminum alloys additionally depends on the critical stress to nucleate a gas bubble. In steel, dissolved gas contents are usually low, so hot tears usually refill with segregated liquid without opening into cracks. This macrosegregation is very damaging, so it becomes a very important phenomenon to model accurately. Every criterion depends on experimental measurements and how best to incorporate them.

Thermal-Analysis-Based Criteria. The results of the solidification heat-transfer analysis alone can provide some important insights into hot tearing. As illustrated in Fig. 2, the location of hot-tear cracks observed in a casting can be related to their time of formation. Cracks tend to initiate near the casting surface (x_1) and propagate toward the center of casting (x_2) as solidification progresses. Figure 2(b) shows the progress of the mushy zone and important isotherms with time, based on the results of a solidification heat-transfer model. In the case of continuous casting, the time axis also corresponds to distance in the casting direction, so the figure depicts the actual shape of the solidification fronts in the real caster.

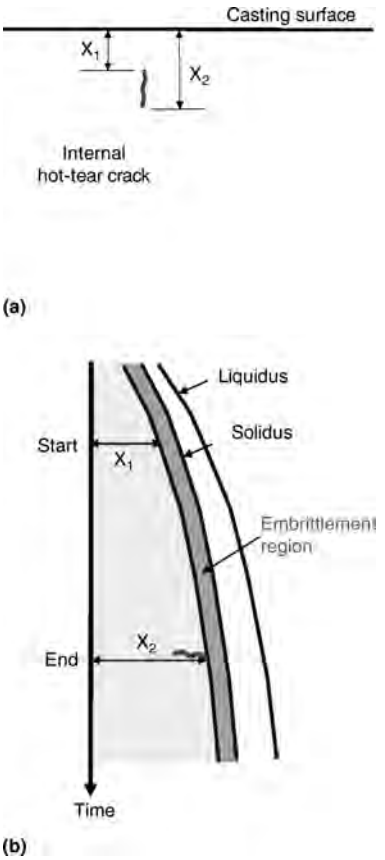

Fig. 2 Relating the location of hot-tear crack formation to results of a transient thermal simulation. (a) Measure crack location in casting. (b) Predict shell thickness history

Casting conditions that produce faster solidification and alloys with wider freezing ranges are more prone to hot tears. Thus, many criteria to indicate hot-tear cracking susceptibility (HCS) are solely based on thermal analysis. One (Ref 73) simply compares the local time spent between two critical solid fractions, g_{s1} and g_{s2} (typically 0.9 and 0.99, respectively), with the total local solidification time (or a reference solidification time):

$$\mathrm{HCS}_{\mathrm{clyne}} = \frac{t_{0.99} - t_{0.90}}{t_{0.90} - t_{0.40}} \quad \text{(Eq 9)}$$

Mechanical-Analysis-Based Criteria. Many different criteria have been developed to predict hot-tear cracks from the results of a mechanical analysis. Regardless of the model formulation, developing an accurate criterion function to predict hot tears relies on measurements, such as the submerged split-chill tensile test (Ref 74–76). This experiment applies and measures a tensile load on the solidifying shell, perpendicular to the growth direction, so it matches the conditions present in hot tearing between columnar grains. Other experiments, such as the Gleeble, apply a tensile load to remelted metal that is held in place by surface tension. Care must be taken in the interpretation of such measurements because the load is generally applied in the same direction as solidification-front growth. Proper interpretation of any hot-tearing experiment requires detailed modeling of the experiment itself, because conditions are never constant, and, at best, only raw data such as temperature, displacement, and force can be measured. The parameters of greatest interest must be extracted using models.

Criteria based on classical mechanics often assume cracks will form when a critical stress is exceeded, and they are popular for predicting cracks at lower temperatures (Ref 77–80). Tensile stress is also a requirement for hot-tear formation (Ref 81). This critical stress depends greatly on the local temperature and strain rate. The maximum tensile stress occurs just before formation of a critical flaw (Ref 82).

Measurements often correlate hot-tear formation with the accumulation of a critical level of mechanical strain while applying tensile loading within a critical solid fraction where liquid feeding is difficult. This has formed the basis for many hot-tearing criteria. One such model (Ref 81) accumulates inelastic deformation over a brittleness temperature range, which is defined, for example, as $g_s \in [0.85, 0.99]$ for a Fe-0.15wt%C steel grade. The local condition for fracture initiation is then:

$$\sum_{g_{s1}}^{g_{s2}} \Delta\varepsilon^{\mathrm{in}} \geq \varepsilon_{\mathrm{cr}} \quad \text{(Eq 10)}$$

in which the critical strain, $\varepsilon_{\mathrm{cr}}$, is 1.6% at a typical strain rate of 3×10^{-4} s^{-1}. Careful measurements during bending of solidifying steel ingots have revealed critical strains ranging from 1 to 3.8% (Ref 81, 83). The lowest values were found at high strain rate and in crack-sensitive grades (e.g., high-sulfur peritectic steel) (Ref 81). In aluminum-rich aluminum-copper alloys, critical strains were reported from 0.09 to 1.6% and were relatively independent of strain rate (Ref 82).

The critical strain decreases with increasing strain rate, presumably because less time is available for liquid feeding, and also decreases for alloys with wider freezing ranges. The following empirical equation for the critical strain in steel, $\varepsilon_{\mathrm{cr}}$, was based on fitting measurements from many bend tests (Ref 84):

$$\varepsilon_{\mathrm{cr}} = \frac{0.02821}{\dot{\varepsilon}^{0.3131} \Delta T_{\mathrm{B}}^{0.8638}} \quad \text{(Eq 11)}$$

where $\dot{\varepsilon}$ is the strain rate (s^{-1}) and ΔT_B is the brittle temperature range (°C) defined between the temperatures corresponding to solid fractions of 0.9 and 0.99.

An elegant analytical-criterion model has been derived to predict hot tearing, based on when the local liquid feeding rate along the interdendritic spaces between the primary columnar dendrites is insufficient to balance the rate of tensile strain increase in the perpendicular direction across the mushy zone (Ref 85, 86). Specifically, gas pores cavitate to separate the residual liquid film between the dendrites when the tensile strain rate exceeds a critical value:

$$\dot{\varepsilon} \geq \frac{1}{R}\left[\frac{\lambda_2^2 \|\nabla T\|}{180\mu_{\mathrm{l}}} \frac{\rho_{\mathrm{L}}}{\rho_{\mathrm{S}}} (p_{\mathrm{m}} - p_{\mathrm{C}}) - \boldsymbol{v}_{\mathrm{T}} \frac{\rho_{\mathrm{S}} - \rho_{\mathrm{L}}}{\rho_{\mathrm{S}}} H\right] \quad \text{(Eq 12)}$$

in which μ_{l} is the dynamic liquid viscosity, λ_2 is the secondary dendrite arm spacing, p_{m} is the local pressure in the liquid ahead of the mushy zone, p_{C} is the cavitation pressure, v_T is the velocity of the solidification front, and $\|\nabla T\|$ is the magnitude of the temperature gradient across the mushy zone. The quantities R and H depend on the solidification path of the alloy:

$$R = \int_{T_2}^{T_1} \frac{g_{\mathrm{s}}^2 F(T)}{g_{\mathrm{l}}^3} dT \quad H = \int_{T_2}^{T_1} \frac{g_{\mathrm{s}}^2}{g_{\mathrm{l}}^2} dT$$
$$F(T) = \frac{1}{\|\nabla T\|} \int_{T_2}^{T} g_{\mathrm{s}} dT \quad \text{(Eq 13)}$$

where the integration limits are calibration parameters (Ref 87). The upper limit T_1 may be the liquidus or the coherency temperature, while the lower limit T_2 typically is within the solid fraction range of 0.95 to 0.99 (Ref 88).

This criterion model has been applied to hot tearing of aluminum microstructures (Ref 87).

For hot tearing within large mushy regions, typically equiaxed microstructures, constitutive behavior of the mushy zone to predict the local fluid flow and deformation of the dendritic network presents an important additional challenge. Other criterion models that focus more on this aspect of hot tearing have recently been developed (Ref 88–90). Further details on hot tearing of aluminum alloys are reviewed elsewhere (Ref 91).

Microscale Model-Based Criteria. Detailed computational models can be developed based on temperature, fluid flow, stress, and strain in the mushy zone during solidification. For example, a finite-element model of an equiaxed mushy zone of aluminum has been applied to investigate constitutive behavior and to quantify strain concentration in the liquid films for a few specific sets of conditions (Ref 92). Once such models are more mature, their results can be incorporated into better criteria for hot tearing. A final difficult task is extracting results from the macroscale model results to compare with the criterion models, owing to the sensitivity of numerical estimates of parameters such as strain rate to numerical oscillations and mesh refinement effects. Thus, coupling difficulties between the macro- and microscale models is another reason that hot-tear crack prediction is an ongoing challenge.

Microsegregation Modeling

Quantifying the relationship between temperature and phase fractions is an essential part of each model involved in the prediction of hot tearing, including the heat transfer, the mechanical, and the hot-tear criterion models. This relationship determines how latent heat is evolved in the heat-transfer model and how to switch between constitutive models in the mechanical model. Although simple linear, lever-rule, or Scheil-based relations are usually sufficient for these macroscale models, microsegregation is an essential aspect of embrittlement and greatly affects the phase-fraction temperature relationship involved in any hot-tearing criterion. Better relationships use the results of microsegregation models that consider partial diffusion of multiple solute elements in the solid phase, using simple analytical solutions (Ref 93), or one-dimensional models of a single secondary dendrite arm (Ref 94). More advanced models couple this calculation together with the macroscale models and allow the relationship to evolve to incorporate nucleation undercooling and other phenomena (Ref 27). Ideally, the relationships applied between dendrites and at grain boundaries should be different, and they should vary with location in the casting, to account for macrosegregation and other phenomena. An important concept, which is often overlooked, is that the same (or very close) relationship must be used in each model of the analysis. Inconsistency between microsegregation models is one of the main reasons why different researchers have proposed different critical temperatures in their hot-tear criteria. Experiments conducted to quantify the parameters in hot-tearing models should fully report both the raw data and the models used to extract hot-tearing parameters, including the microsegregation model.

Model Validation

Model validation is a crucial step in any computational analysis. Analytical solutions are needed to prove internal consistency of the model and to control discretization errors. Comparison with experiments is needed to prove the model assumptions, property data, and boundary conditions. Weiner and Boley (Ref 95) derived an analytical solution for unidirectional solidification of an unconstrained plate, which serves as an ideal benchmark problem to validate thermal and mechanical models. The plate is subjected to sudden surface quench from a uniform initial temperature to a constant mold temperature, with a unique solidification temperature, an elastic-perfectly-plastic constitutive law, and constant properties.

This benchmark problem can be solved with a simple mesh of one row of elements extending from the casting surface into the liquid, as shown in Fig. 3. Numerical predictions should match with acceptable precision using the same element type, mesh refinement, and time steps planned for the real problem. For example, the solidification stress analysis code CON2D (Ref 55) and the commercial code ABAQUS (Ref 51) were applied for typical conditions of steel casting (Ref 56).

Figures 4 and 5 compare the temperature and stress profiles in the plate at two times. The temperature profile through the solidifying shell is almost linear. Because the interior cools relative to the fixed surface temperature, its shrinkage generates internal tensile stress, which induces compressive stress at the surface. With no applied external pressure, the average stress through the thickness must naturally equal zero, and stress must decrease to zero in the liquid. Stresses and strains in both transverse directions are equal for this symmetrical problem. The close agreement demonstrates that the computational model is numerically consistent and has an acceptable mesh resolution. Such studies reveal that a relatively fine mesh is needed to achieve reasonable accuracy, and that results from many thermomechanical models reported in previous literature had insufficient mesh refinement. Comparison with experimental measurements is also required, to validate that the modeling assumptions and input data are reasonable.

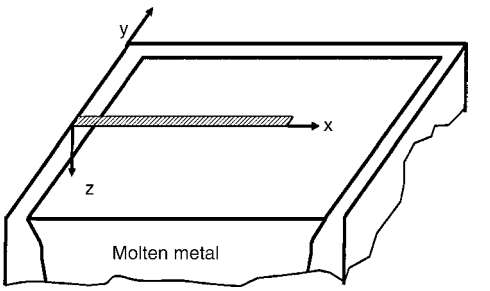

Fig. 3 One-dimensional slice domain for modeling solidifying plate

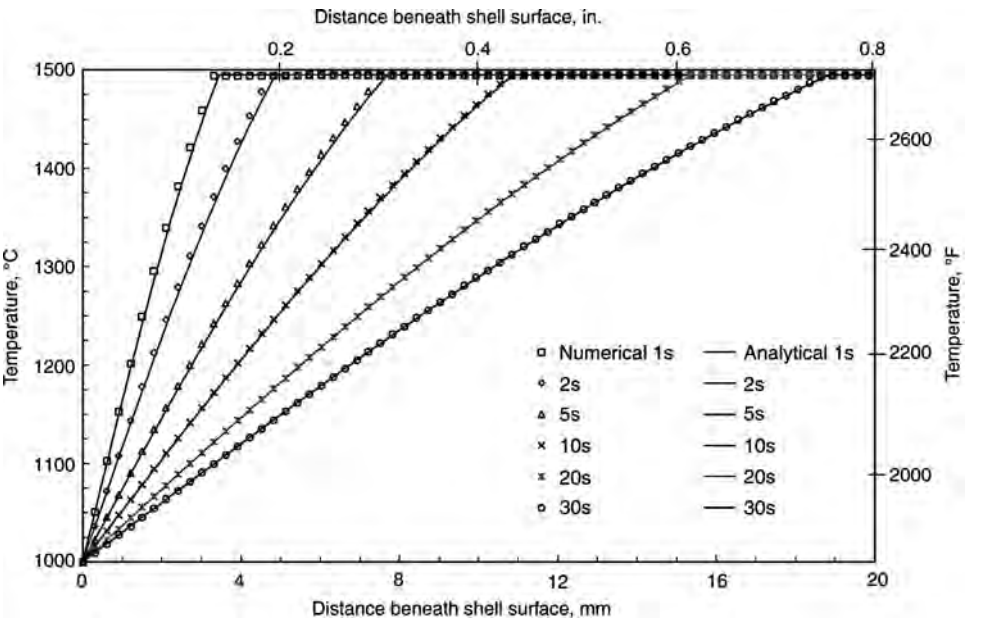

Fig. 4 Temperatures through solidifying plate at different times, comparing analytical solution and numerical predictions

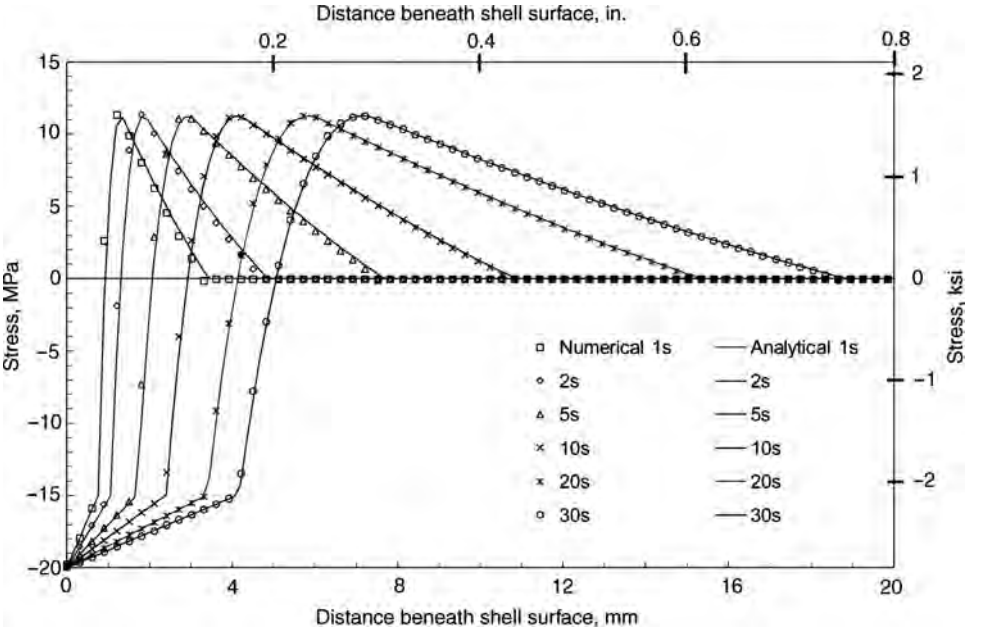

Fig. 5 Lateral (*y* and *z*) stress through solidifying plate at different times, comparing analytical solution and numerical predictions

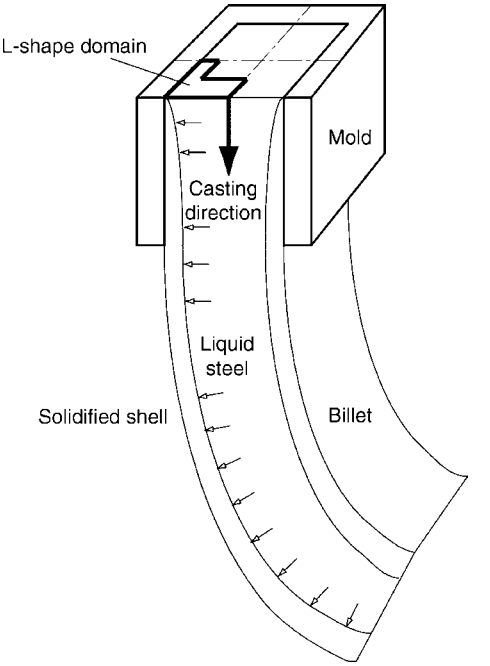

Fig. 6 Model domain

Case Study—Billet Casting Speed Optimization

A Lagrangian model of temperature, distortion, strain, stress, and hot tearing has been applied to predict the maximum speed for continuous casting of steel billets without forming off-corner internal hot-tear cracks. The two-dimensional transient finite-element thermomechanical model, CON2D (Ref 55, 56), has been used to track a transverse slice through the solidifying steel strand as it moves downward at the casting speed to reveal the entire three-dimensional stress state. The two-dimensional assumption produces reasonable temperature predictions, because axial (*z*-direction) conduction is negligible relative to axial advection (Ref 43). In-plane mechanical predictions are also reasonable, because bulging effects are small, and the undiscretized casting direction is modeled with the appropriate condition of generalized plain strain. Other applications with this model include the prediction of ideal taper of the mold walls (Ref 96) and quantifying the effect of steel grade on oscillation mark severity during level fluctuations (Ref 97).

The model domain is an L-shaped region of a two-dimensional transverse section, shown in Fig. 6. Removing the central liquid region saves computation and lessens stability problems related to element locking. Physically, this "trick" is important in two-dimensional domains because it allows the liquid volume to change without generating stress, which mimics the effect of fluid flow into and out of the domain that occurs in the actual open-topped casting process. Simulations start at the meniscus, 100 mm below the mold top, and extend through the 800 mm long mold and below, for a caster with no submold support. The instantaneous heat flux, given in Eq 14, was based on plant measurements (Ref 98). It was assumed to be uniform around the perimeter of the billet surface in order to simulate ideal taper and perfect contact between the shell and mold. Below the mold, the billet surface temperature was kept constant at its circumferential profile at mold exit. This eliminates the effect of spray cooling practice imperfections on submold reheating or cooling and the associated complication for the stress/strain development. A typical plain carbon steel was studied (0.27% C, 1.52% Mn, 0.34% Si) with 1500.7 °C liquidus temperature and 1411.8 °C solidus temperature:

$$q\left(\mathrm{MW/m^2}\right) = \begin{cases} 5 - 0.2444t(\mathrm{s}) & t \le 1.0\ \mathrm{s} \\ 4.7556t(\mathrm{s})^{-0.504} & t > 1.0\ \mathrm{s} \end{cases} \quad \text{(Eq 14)}$$

Different constitutive models were used for each phase of the solidifying steel. The following elastic-visco-plastic constitutive equation was developed for the austenite phase (Ref 99) as a function of percent carbon content (%C) by fitting constant strain-rate tensile tests (Ref 100, 101) and constant-load creep tests (Ref 102) to the form in Eq 5 and 7:

$$\dot{\varepsilon}_{eq} = f_{\%\mathrm{C}} \left\langle \sigma_{\mathrm{eq}} - \sigma_0 \right\rangle^{1/m} \exp\left(-\frac{4.465\times10^4}{T}\right)$$

where

$$\begin{aligned} f_{\%\mathrm{C}} &= 4.655 \times 10^4 + 7.14 \times 10^4 (\%\mathrm{C}) \\ &\quad + 1.2 \times 10^4 (\%\mathrm{C})^2 \\ \sigma_0 &= (130.5 - 5.128 \times 10^{-3} T)\varepsilon_{eq}^{f_2} \\ f_2 &= -0.6289 + 1.114 \times 10^{-3} T \\ 1/m &= 8.132 - 1.54 \times 10^{-3} T \end{aligned} \quad \text{(Eq 15)}$$

with T in kelvin, and σ_{eq} and σ_0 in MPa

Further equations, such as the associated flow rule, are needed to transform this scalar equation into tensor form and to account for reversals in loading conditions. Equation 15 and a similar one for delta-ferrite have been implemented into the finite-element codes CON2D (Ref 55) and THERCAST (Ref 103) and applied to investigate several problems involving mechanical behavior during continuous casting.

Elastic modulus is a crucial property that decreases with increasing temperature. It is difficult to measure at the high temperatures important to casting, owing to the susceptibility of the material to creep and thermal strain during a standard tensile test, which results in excessively low values. Higher values are obtained from high-strain-rate tests, such as ultrasonic measurements (Ref 104). Elastic modulus measurements in steels near the solidus temperature range from ~1 (Ref 105) to 44 GPa (Ref 106), with typical modulus values of ~10 GPa near the solidus (Ref 98, 107, 108).

The density needed to compute thermal strain in Eq 8 can be found from a weighted average of the values of the different solid and liquid phases, based on the local phase fractions. For the example of plain low-carbon steel, the following equations were compiled (Ref 55) based on the phase fractions of alpha-ferrite (f_α), austenite (f_γ), delta-ferrite (f_δ) (Ref 109, 110), and liquid (f_l) measurements (Ref 111):

$$\begin{aligned}\rho\left(\mathrm{kg/m^3}\right) &= \rho_\alpha f_\alpha + \rho_\gamma f_\gamma + \rho_\delta f_\delta + \rho_l f_l \\ \rho_\alpha &= 7881 - 0.324T(^\circ\mathrm{C}) - 3\times 10^{-5}T(^\circ\mathrm{C})^2 \\ \rho_\gamma &= \frac{100[8106 - 0.51T(^\circ\mathrm{C})]}{[100 - (\%\mathrm{C})][1 + 0.008(\%\mathrm{C})]^3} \\ \rho_\delta &= \frac{100[8011 - 0.47T(^\circ\mathrm{C})]}{[100 - (\%\mathrm{C})][1 + 0.013(\%\mathrm{C})]^3} \\ \rho_l &= 7100 - 73(\%\mathrm{C}) - [0.8 - 0.09(\%\mathrm{C})] \\ &\quad [T(^\circ\mathrm{C}) - 1550]\end{aligned} \tag{Eq 16}$$

Sample results are presented here for one-quarter of a 120 mm square billet cast at speeds of 2.0 and 5.0 m/min. The latter is the critical speed at which hot-tear crack failure of the shell is just predicted to occur. The temperature and axial (z) stress distributions in a typical section through the wideface of the steel shell cast at 2.0 m/min are shown in Fig. 7 and Fig. 8 at four different times during cooling in the mold. Unlike the analytical solution in Fig. 4, the surface temperature drops as time progresses. The corresponding stress distributions are qualitatively similar to the analytical solution (Fig. 5). The stresses increase with time, however, as solidification progresses. The realistic constitutive equations produce a large region of tension near the solidification front. The magnitude of these stresses (and the corresponding strains) are not predicted to be enough to cause hot tearing in the mold, however. The results from two different codes reasonably match, demonstrating that the formulations are accurately implemented, convergence has been achieved, and that the mesh and time-step refinement are sufficient.

Figure 9(a) shows the distorted temperature contours near the strand corner at 200 mm below the mold exit for a casting speed of 5.0 m/min. The corner region is coldest, owing to two-dimensional cooling. The shell becomes hotter and thinner with increasing casting speed, owing to less time in the mold. This weakens the shell, allowing it to bulge more under the ferrostatic pressure below the mold.

Figure 9(b) shows contours of hoop stress constructed by taking the stress component acting perpendicular to the dendrite growth direction, which simplifies to σ_x in the lower right portion of the domain and σ_y in the upper left portion. High values appear at the off-corner subsurface region, due to a hinging effect that the ferrostatic pressure over the entire face exerts around the corner. This bends the shell around the corner and generates high subsurface tensile stress at the weak solidification front in the off-corner subsurface location. This tensile stress peak increases slightly and moves toward the surface at higher casting speed. Stress concentration is less and the surface hoop stress is compressive at the lower casting speed. This indicates no possibility of surface cracking. However, tensile surface hoop stress is generated below the mold at high speed in Fig. 9(b) at the face center due to excessive bulging. This tensile stress, and the accompanying hot-tear strain, may contribute to longitudinal cracks that penetrate the surface.

Hot tearing was predicted using the criterion in Eq 10 with the critical strain given in Eq 11. Inelastic strain was accumulated for the component oriented normal to the dendrite growth direction, because that is the weakest direction and corresponds to the measurements used to obtain Eq 11. Figure 9(c) shows contours of hot-tear strain in the hoop direction. The highest values appear at the off-corner subsurface region in the hoop direction. Moreover, significantly higher values are found at higher casting speeds. For this particular example, hot-tear strain exceeds the threshold at 12 nodes, all located near the off-corner subsurface region. This is caused by the hinging mechanism

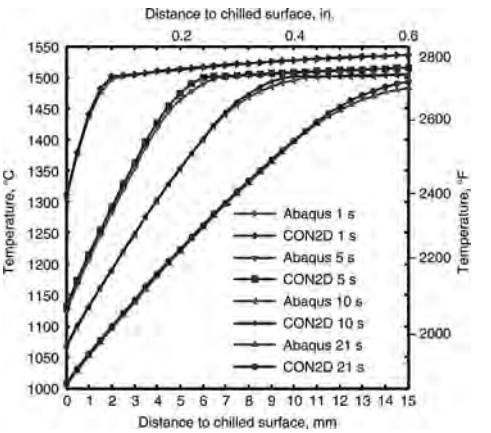

Fig. 7 Temperature distribution along the solidifying slice in continuous casting mold

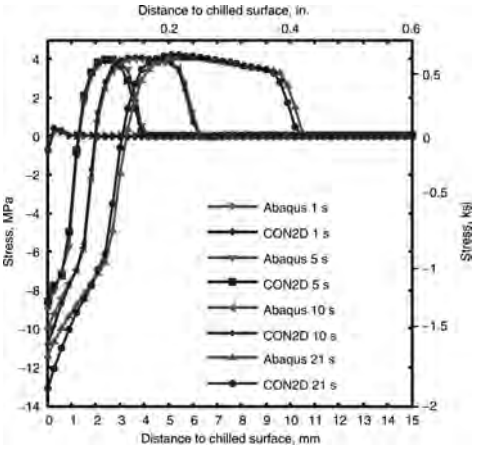

Fig. 8 Lateral (y and z) stress distribution along the solidifying slice in continuous casting mold

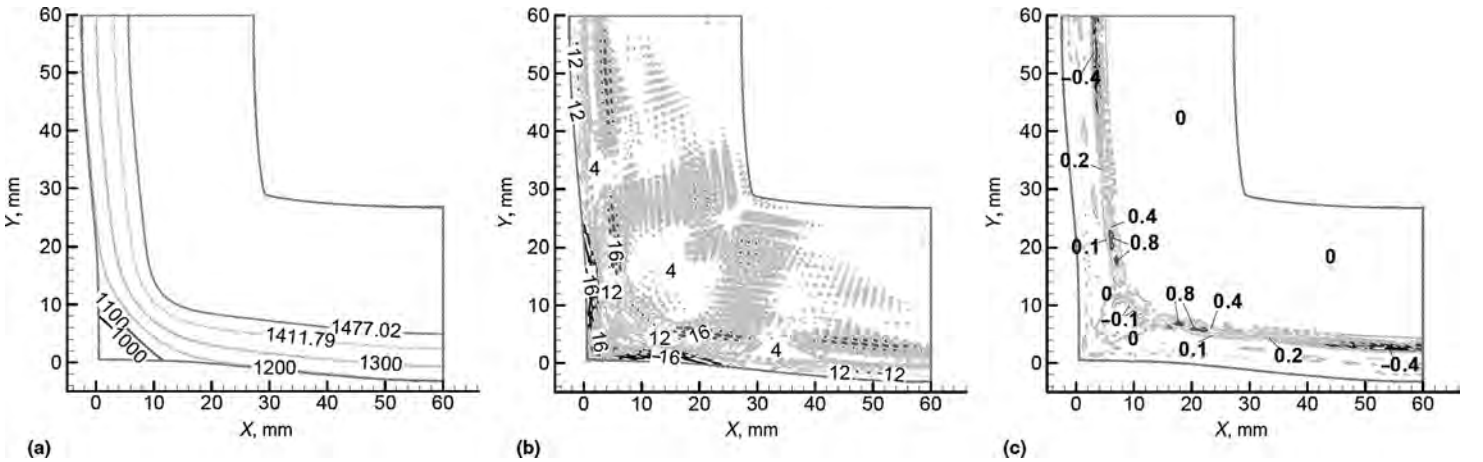

Fig. 9 Distorted contours at 200 mm below mold exit. (a) Temperature. (b) Hoop stress. (c) Hot-tear strain

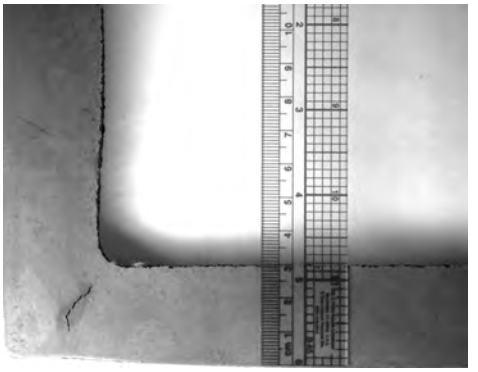

Fig. 10 Off-corner internal hot-tear crack in break-out shell from a 175 mm square bloom

around the corner. No nodes fail at the center surface, in spite of the high tensile stress there. The predicted hot-tearing region matches the location of off-corner longitudinal cracks observed in sections through real solidifying shells, such as the one pictured in Fig. 10. The bulged shape is also similar.

Results from many computations were used to find the critical speed to avoid hot-tear cracks as a function of section size and working mold length, as presented in Fig. 11 (Ref 108). These predictions slightly exceed plant practice, which is generally chosen by empirical trial and error. This suggests that plant conditions such as mold taper are less than ideal, that other factors limit casting speed, or those speeds in practice could be increased. The qualitative trends are the same.

This quantitative model of hot tearing provides many useful insights into the continuous casting process. Larger section sizes are more susceptible to bending around the corner and thus have a lower critical speed, resulting in less productivity increase than expected. The trend toward longer molds over the past three decades enables a higher casting speed without cracks by producing a thicker, stronger shell at mold exit.

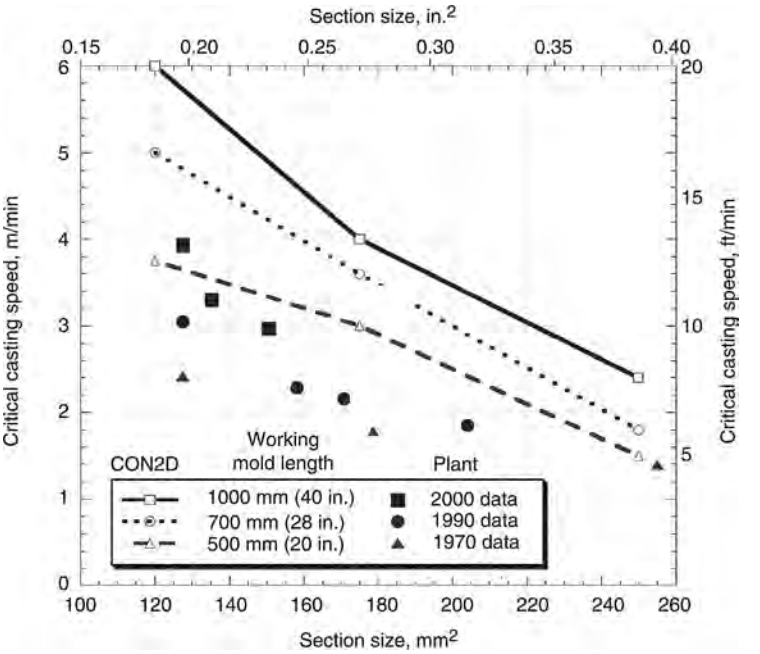

Fig. 11 Comparison of critical casting speeds, based on hot-tearing criterion and typical plant practice. Source: Ref 112

Conclusions

The prediction of defects represents the culmination of solidification modeling. It enables models to make practical contributions to real commercial processes, but it requires incorporating together and augmenting the models of almost every other aspect of casting simulation. Hot-tear crack prediction requires accurate thermal and mechanical analysis, combined with criteria for embrittlement. As computing power and software tools for computational mechanics advance, it is becoming increasingly possible to perform useful analysis of fluid flow, temperature, deformation, strain, stress, and related phenomena in real casting processes. Computations are still hampered by the limits of mesh resolution and computational speed, especially for realistic three-dimensional geometries and defect analysis. The modeling of defects such as hot tears is still in its infancy, and there is much work to be done.

ACKNOWLEDGMENTS

The author wishes to thank the member companies of the Continuous Casting Consortium, the National Center for Supercomputing Applications at the University of Illinois, and the National Science Foundation for support of this work. Thanks are also extended to Michel Bellet, Ecole des Mines de Paris, for coauthoring a previous version of this article, which appeared in *Casting*, Volume 15 *ASM Handbook*, 2008 (Ref 72), upon which this article is based.

REFERENCES

1. L. Zhang, B.G. Thomas, X. Wang, and K. Cai, Evaluation and Control of Steel Cleanliness—A Review, *Steelmaking Conf. Proc.,* Vol 85, March 10–13, 2002 (Nashville, TN), ISS, Warrendale, PA, 2002, p 431–452.
2. A. Ashrafian and S.T. Johansen, Special Issue: CFD Applications in Metallurgical and Process Industries—Preface, *Progress in Computational Fluid Dynamics,* Vol 7 (2–4), 2007, p 69.
3. FLUENT6.2, Ansys Inc., 10 Cavendish Court, Lebanon, NH, 2009.
4. S.T. Johansen and F. Boysan, Fluid-Dynamics in Bubble Stirred Ladles. 2. Mathematical Modeling, *Metall. Mater. Trans. B—Process Metallurgy,* Vol 19 (5), 1988, p 755–764.
5. B.G. Thomas, Q. Yuan, S. Sivaramakrishnan, T. Shi, S.P. Vanka, and M.B. Assar, Comparison of Four Methods to Evaluate Fluid Velocities in a Continuous Slab Casting Mold, *ISIJ Int. (Japan),* Vol 41 (10), 2001, p 1262–1271.
6. Q. Yuan, B. Zhao, S.P. Vanka, and B.G. Thomas, Study of Computational Issues in Simulation of Transient Flow in Continuous Casting, *Steel Res. Int.,* Vol 76 (1, Special Issue: Simulation of Fluid Flow in Metallurgy), 2005, p 33–43.
7. Q. Yuan, S. Sivaramakrishnan, S.P. Vanka, and B.G. Thomas, Computational and Experimental Study of Turbulent Flow in a 0.4-Scale Water Model of a Continuous Steel Caster, *Metall. Mater. Trans.,* Vol 35B (5), 2004, p 967–982.
8. B. Sundman, B. Jansson, and J.-O. Andersson, The Thermo-Calc Databank System, *Calphad,* Vol 9, 1985, p 153–190.
9. A.D. Pelton, C.W. Bale, G. Eriksson, K. Hack, S. Petersen, and P. Koukkari, Demonstration of FACTSage and ChemApp at HTMC-X, *High Temperature Materials Chemistry, Abstracts of the Tenth International IUPAC Conference*, K. Hilpert, F.W. Froben, and L. Singheiser, Ed., April 10–14, 2000 (Jülich, Germany), 2000, p 77.
10. A.T. Dinsdale, S.M. Hodson, T.I. Barry, and J.R. Taylor, Computations Using MTDATA of Metal-Matte-Slag-Gas

Equilibria, *Computer Software in Chemical and Extractive Metallurgy,* Pergamon Press, New York, NY, 1989, p 59–74.
11. B. Cheynet, Complex Chemical Equilibria Calculations with the THERMODATA System, *Computer Software in Chemical and Extractive Metallurgy,* Pergamon Press, New York, NY, 1989, p 31–44.
12. A.W. Cramb, Y. Chung, J. Harman, A. Sharan, and I. Jimbo, The Slag/Metal Interface and Associated Phenomena. A History of Pneumatic Steelmaking, *Iron Steelmaker (USA),* Vol 24 (3), 1997, p 77–83.
13. L. Wang and C. Beckermann, Prediction of Reoxidation Inclusion Composition in Casting of Steel, *Metall. Mater. Trans. B—Process Metallurgy and Materials Processing Science,* Vol 37 (4), 2006, p 571–588.
14. B.G. Thomas and L. Zhang, Review: Mathematical Modeling of Fluid Flow in Continuous Casting, *ISIJ Int.,* Vol 41 (10), 2001, p 1181–1193.
15. Q. Yuan, B.G. Thomas, and S.P. Vanka, Study of Transient Flow and Particle Transport during Continuous Casting of Steel Slabs, Part 2: Particle Transport, *Metall. Mater. Trans. B.,* Vol 35B (4), 2004, p 703–714.
16. L. Zhang, J. Aoki, and B.G. Thomas, Inclusion Removal by Bubble Flotation in a Continuous Casting Mold, *Metall. Mater. Trans. B,* Vol 37B, 2006, p 361–379.
17. T. Nakaoka, S. Taniguchi, K. Matsumoto, and S.T. Johansen, Particle-Size-Grouping Method of Inclusion Agglomeration and Its Application to Water Model Experiments, *ISIJ Int.,* Vol 41 (10), 2001, p 1103–1111.
18. L. Zhang and S. Taniguchi, Fundamentals of Inclusions Removal from Liquid Steel by Bubbles Flotation, *Int. Mater. Rev.,* Vol 45 (2), 2000, p 59–82.
19. K.G. Rackers and B.G. Thomas, Clogging in Continuous Casting Nozzles, *Continuous Casting,* Vol 10, *Tundish Operations,* Iron and Steel Society, Warrendale, PA, 2003, p 264–274.
20. A.V. Catalina, S. Mukherjee, and D.M. Stefanescu, A Dynamic Model for the Interaction between a Solid Particle and an Advancing Solid/Liquid Interface, *Metall. Mater. Trans. A,* Vol 31A (10), 2000, p 2559–2568.
21. Q. Yuan and B.G. Thomas, Transport and Entrapment of Particles in Continuous Casting of Steel, *Third Int. Congress on Science and Technology of Steelmaking,* May 9–11, 2005 (Charlotte, NC), Association for Iron and Steel Technology, Warrendale, PA, 2005, p 745–762.
22. M. Serriere, C.A. Gandin, E. Gautier, P. Archambault, and M. Dehmas, Modeling of Precipitation Coupled with Thermodynamic Calculations, *Aluminum Alloys 2002: Their Physical and Mechanical Properties Pts 1–3,* Vol 396-4, 2002, p 747–752.
23. G. Lesoult, C.A. Gandin, and N.T. Niane, Segregation during Solidification with Spongy Deformation of the Mushy Zone, *Acta Mater.,* Vol 51, 2003, p 5263–5283.
24. K. Miyazawa and K. Schwerdtfeger, Macrosegregation in Continuously Cast Steel Slabs: Preliminary Theoretical Investigation on the Effect of Steady State Bulging, *Arch. Eisenhutten,* Vol 52 (11), 1981, p 415–422.
25. A.F. Giamei and B.H. Kear, On the Nature of Freckles in Nickel Base Superalloys, *Metall. Trans.,* Vol 1, 1970, p 2185–2192.
26. H.J. Thevik, A. Mo, and T. Rusten, A Mathematical Model for Surface Segregation in Aluminum Direct Chill Casting, *Metall. Mater. Trans. B—Process Metallurgy and Materials Processing Science,* Vol 30 (1), 1999, p 135–142.
27. C. Beckermann, Modelling of Macrosegregation: Applications and Future Needs, *Int. Mater. Rev.,* Vol 47 (5), 2002, p 243–262.
28. J.A. Dantzig and M. Rappaz, *Solidification,* Taylor and Francis, EPFL Publishing, 2009, p 250.
29. M.C. Flemings and G.E. Nereo, Macrosegregation, *Trans. AIME,* Vol 239, 1967, p 1449–1461.
30. E. Niyama, T. Uchida, M. Morikawa, and S. Saito, Method of Shrinkage Prediction and Its Application to Steel Casting Practice, *AFS Int. Cast Metals J.,* Vol 7, 1982, p 52–63.
31. K.D. Carlson and C. Beckermann, Prediction of Shrinkage Pore Volume Fraction Using a Dimensionless Niyama Criterion, *Metall. Mater. Trans. A—Physical Metallurgy and Materials Science,* Vol 40A (1), 2009, p 163–175.
32. K.D. Carlson, Z.P. Lin, C. Beckermann, G. Mazurkevich, and M. Schneider, Modeling of Porosity Formation in Aluminum Alloys, *Aluminium Alloys 2006, Pts 1 and 2,* Vol 519–521, 2006, p 1699–1706.
33. P.D. Lee, A. Chirazi, and D. See, Modeling Microporosity in Aluminum-Silicon Alloys: A Review, *J. Light Met.,* Vol 1 (1), 2001, p 15–30.
34. K. Venkatesan and R. Shivpuri, Experimental and Numerical Investigation of the Effect of Process Parameters on the Erosive Wear of Die-Casting Dies, *J. Mater. Eng. Perform.,* Vol 4 (2), 1995, p 166–174.
35. K. Domkin, J. Thorborg, and J. Hattel, Modeling of High-Temperature and Diffusion-Controlled Die Soldering in Aluminum High-Pressure Die Casting, *J. Mater. Process. Technol.,* 2008, in press.
36. Q. Han and S. Viswanathan, Analysis of the Mechanism of Die Soldering in Aluminum Die Casting, *Metallurg. Mater. Trans. A,* Vol 34 (1), 2003, p 139–146.
37. S. Shankar and D. Apelian, Die Soldering: Mechanism of the Interface Reaction between Molten Aluminum Alloy and Tool Steel, *Metall. Mater. Trans. B,* Vol 33 (3), 2002, p 465–476.
38. J.-K. Park, B.G. Thomas, I.V. Samarasekera, and U.-S. Yoon, Thermal and Mechanical Behavior of Copper Moulds during Thin Slab Casting (II): Mould Crack Formation, *Metall. Mater. Trans.,* Vol 33B, June 2002, p 437–449.
39. T. O'Conner and J. Dantzig, Modeling the Thin Slab Continuous Casting Mold, *Metall. Mater. Trans. B,* Vol 25B (4), 1994, p 443–457.
40. M. Asta, C. Beckermann, A. Karma, W. Kurz, R. Napolitano, M. Plapp, G. Purdy, M. Rappaz, and R. Trivedi, Solidification Microstructures and Solid-State Parallels: Recent Developments, Future Directions, *Acta Mater.,* Vol 57 (4), 2009, p 941–971.
41. W.A. Curtin and R.E. Miller, Atomistic/Continuum Coupling in Computational Materials Science, *Model. Simul. Mater. Sci. Eng.,* Vol 11 (3), 2003, p R33–R68.
42. J.E. Kelly, K.P. Michalek, T.G. O'Connor, B.G. Thomas, and J.A. Dantzig, Initial Development of Thermal and Stress Fields in Continuously Cast Steel Billets, *Metall. Trans. A,* Vol 19A (10), 1988, p 2589–2602.
43. Y. Meng and B.G. Thomas, Heat Transfer and Solidification Model of Continuous Slab Casting: CON1D, *Metall.Mater. Trans.,* Vol 34B (5), 2003, p 685–705.
44. C.V. Madhusudana and L.S. Fletcher, Contact Heat Transfer—The Last Decade, *AIAA J.,* Vol 24, 1985, p 510–523.
45. G.E. Mase and G.T. Mase, *Continuum Mechanics for Engineers*, 2nd ed., CRC Press, 1999.
46. Y. Estrin, A Versatile Unified Constitutive Model Based on Dislocation Density Evolution, *Constitutive Modelling— Theory and Application*, Vol MD-Vol 26/AMD-Vol 121, ASME, New York, 1991, p 65–75.
47. C. Agelet de Saracibar, M. Cervera, and M. Chiumenti, On the Constitutive Modeling of Coupled Thermomechanical Phase-Change Problems, *Int. J. Plast.,* Vol 17, 2001, p 1565–1622.
48. J. Sengupta, S.L. Cockcroft, D.M. Maijer, and A. Larouche, Quantification of Temperature, Stress, and Strain Fields during the Start-Up Phase of Direct Chill Casting Process by Using a 3-D Fully Coupled Thermal and Stress Model for AA5182 Ingots, *Mater. Sci. Eng. A,* Vol 397, 2005, p 157–177.
49. A.E. Huespe, A. Cardona, and V. Fachinotti, Thermomechanical Model of a Continuous Casting Process, *Computer Methods in Appl. Mech. Engr.,* Vol 182 (3), 2000, p 439–455.
50. *MARC Users Manual,* MARC Analysis Research Corp., Palo Alto, CA, 1991.
51. "ABAQUS Theory Manual v6.0," Abaqus, Inc., Pawtucket, RI, 2004.

52. A. Hakonsen and D. Mortensen, *Modeling of Casting, Welding and Advanced Solidification Processes VII,* The Minerals, Metals and Materials Society, Warrendale, PA, 1995, p 963–970.
53. H.G. Fjaer and A. Mo, ALSPEN—A Mathematical Model for Thermal Stresses in DC-Cast Al Billets, *Metall. Trans.,* Vol 21B (6), 1990, p 1049–1061.
54. G. Laschet, J. Jakumeit, and S. Benke, Thermo-Mechanical Analysis of Cast/Mould Interaction in Casting Processes, *Z. Metallkd.,* Vol 95, 2004, p 1087–1096.
55. C. Li and B.G. Thomas, Thermo-Mechanical Finite-Element Model of Shell Behavior in Continuous Casting of Steel, *Metall. Mater. Trans. B.,* Vol 35B (6), 2004, p 1151–1172.
56. S. Koric and B.G. Thomas, Efficient Thermo-Mechanical Model for Solidification Processes, *Int. J. Num. Meths. Eng.,* Vol 66 (12), 2006, p 1955–1989.
57. MAGMASOFT, http://www.magmasoft.com, 2007.
58. PROCAST, Procast, http://www.esi-group.com/SimulationSoftware/Die_Casting_Solution/Products/Casting_simulation/, 2007.
59. M. Samonds and J.Z. Zhu, Coupled Thermal-Fluid-Stress Analysis of Castings, *Proc. MCWASP IX, Ninth Int. Conf. on Modeling of Casting, Welding and Advanced Solidification Processes,* P.R. Sahm, P.N. Hansen, and J.G. Conley, Ed., August 20–25, 2000 (Aachen Germany), Shaker Verlag, Aachen, 2000, p 80–87.
60. J.M. Drezet, A. Bughardt, H.G. Fjaer, and B. Magnin, *Mater. Sci. Forum 2000,* Vol 329–330, 2000, p 493–500.
61. H.G. Fjaer and A. Hakonsen, The Mechanism of Pull-In during DC-Casting of Aluminum Sheet Ingots, *Light Metals 1997,* The Minerals, Metals and Materials Society, Warrendale, PA, 1997, p 683–690.
62. A. Mo, M. Rappaz, and L.L. Martin, *Aluminum,* Vol 78 (10), 2002, p 856–864.
63. A. Henry, *Light Met. Age,* Vol 58 (7–8), 2000, p 66–67.
64. M. Bellet, O. Jaouen, and I. Poitrault, An ALE-FEM Approach to the Thermomechanics of Solidification Processes with Application to the Prediction of Pipe Shrinkage, *Int. J. Num. Meth. Heat Fluid Flow,* Vol 15, 2005, p 120–142.
65. S. Koric, L.C. Hibbeler, and B.G. Thomas, Explicit Coupled Thermo-Mechanical Finite Element Model of Steel Solidification, *Int. J. Num. Meths. Engineering,* 2009, submitted.
66. O.C. Zienkiewicz and R.L. Taylor, *The Finite Element Method,* 4th ed., McGraw Hill, New York, NY, 1988.
67. J.-M. Drezet, B. Commet, H.G. Fjaer, and B. Magnin, Stress-Strain Computations of the DC Casting Process of Aluminum Alloy: A Sensitivity Study on Material Properties, *Proc. MCWASP IX, Ninth Int. Conf. on Modeling of Casting, Welding and Advanced Solidification Processes,* P.R. Sahm, P.N. Hansen, and J.G. Conley, Ed., August 20–25, 2000 (Aachen Germany), Shaker Verlag, Aachen, 2000, p 33–40.
68. X. Huang, B.G. Thomas, and F.M. Najjar, Modeling Superheat Removal during Continuous Casting of Steel Slabs, *Metall. Trans. B,* Vol 23B (6), 1992, p 339–356.
69. M. Bellet and V.D. Fachinotti, ALE Method for Solidification Modelling, *Comput. Methods Appl. Mech. Eng.,* Vol 193, 2004, p 4355–4381.
70. Thercast presentation, www.transvalor.com and www.scconsultants.com, 2007.
71. M. Chiumenti, M. Cervera, and C.A.D. Saracibar, Coupled Thermomechanical Simulation of Solidification and Cooling Phases in Casting Processes, *Proc. MCWASP XI, 11th Int. Conf. on Modeling of Casting, Welding and Advanced Solidification Processes,* C.-A. Gandin and M. Bellet, Ed., The Minerals, Metals and Materials Society, Warrendale, PA, 2006, p 201–208.
72. B.G. Thomas and M. Bellet, Modeling of Stress, Distortion, and Hot Tearing, *Casting*, Vol 15, *ASM Handbook,* S. Viswanathan and E. DeGuire, Ed., ASM International, 2008, p 449–461.
73. T.W. Clyne and G.J. Davies, Comparison between Experimental Data and Theoretical Predictions Relating to Dependence of Solidification Cracking on Composition, *Solidification and Casting of Metals,* The Metals Society, London, 1979, p 275–278.
74. P. Ackermann, W. Kurz, and W. Heinemann, In Situ Tensile Testing of Solidifying Aluminum and Al-Mg Shells, *Mater. Sci. Eng.,* Vol 75, 1985, p 79–86.
75. C. Bernhard, H. Hiebert, and M.M. Wolf, Simulation of Shell Strength Properties by the SSCT Test, *ISIJ Int. (Japan),* Vol 36 (Suppl. Science and Technology of Steelmaking), 1996, p S163–S166.
76. M. Suzuki, C. Yu, and T. Emi, In-Situ Measurement of Tensile Strength of Solidifying Steel Shells to Predict Upper Limit of Casting Speed in Continuous Caster with Oscillating Mold, *ISIJ Int., Iron Steel Inst. Japan,* Vol 37 (4), 1997, p 375–382.
77. K. Kinoshita, T. Emi, and M. Kasai, Thermal Elasto-Plastic Stress Analysis of Solidifying Shell in Continuous Casting Mold, *Tetsu-to-Hagane,* Vol 65 (14), 1979, p 2022–2031.
78. J.O. Kristiansson, Thermal Stresses in the Early Stage of Solidification of Steel, *J. Therm. Stresses,* Vol 5, 1982, p 315–330.
79. B.G. Thomas, I.V. Samarasekera, and J.K. Brimacombe, Mathematical Model of the Thermal Processing of Steel Ingots, Part II: Stress Model, *Metall. Trans. B,* Vol 18B (1), 1987, p 131–147.
80. K. Okamura and H. Kawashima, Calculation of Bulging Strain and Its Application to Prediction of Internal Cracks in Continuously Cast Slabs, *Proc. Int. Conf. Comp. Assoc. Mat. Design Proc. Simul.,* ISIJ, Tokyo, 1993, p 129–134.
81. A. Yamanaka, K. Nakajima, K. Yasumoto, H. Kawashima, and K. Nakai, Measurement of Critical Strain for Solidification Cracking, *Modelling of Casting, Welding, and Advanced Solidification Processes—V,* M. Rappaz, M.R. Ozgu, and K.W. Mahin, Ed. (Davos, Switzerland), TMS, Warrendale, PA, 1990, p 279–284.
82. P. Wisniewski and H.D. Brody, Tensile Behavior of Solidifying Aluminum Alloys, *Modelling of Casting, Welding, and Advanced Solidification Processes— V,* M. Rappaz, M.R. Ozgu, and K.W. Mahin, Ed. (Davos, Switzerland), TMS, Warrendale, PA, 1990, p 273–278.
83. A. Yamanaka, K. Nakajima, and K. Okamura, Critical Strain for Internal Crack Formation in Continuous Casting, *Ironmaking Steelmaking,* Vol 22 (6), 1995, p 508–512.
84. Y.-M. Won, T.J. Yeo, D.J. Seol, and K.H. Oh, A New Criterion for Internal Crack Formation in Continuously Cast Steels, *Metall. Mater. Trans. B,* Vol 31B, 2000, p 779–794.
85. U. Feurer, Mathematisches Modell der Warmrissneigung von Binären Aluminium Legierungen, *Giessereiforschung,* Vol 28, 1976, p 75–80.
86. M. Rappaz, J.-M. Drezet, and M. Gremaud, A New Hot-Tearing Criterion, *Metall. Mater. Trans. A,* Vol 30A (2), 1999, p 449–455.
87. J.M. Drezet and M. Rappaz, Prediction of Hot Tears in DC-Cast Aluminum Billets, *Light Metals*, J.L. Anjier, Ed. TMS, Warrendale, PA, 2001, p 887–893.
88. M. M'Hamdi, S. Benum, D. Mortensen, H. G. Fjaer, and J.M. Drezet, The Importance of Viscoplastic Strain Rate in the Formation of Center Cracks during the Start-Up Phase of Direct-Chill Cast Aluminium Extrusion Ingots, *Metall. Mater. Trans. A,* Vol 34, 2003, p 1941–1952.
89. M. M'Hamdi, A. Mo, and H.G. Fjaer, *Metall. Mater. Trans. A,* Vol 37, 2006, p 3069–3083.
90. V. Mathier, S. Vernede, P. Jarry, and M. Rappaz, Two-Phase Modeling of Hot Tearing in Aluminum Alloys: Applications of a Semicoupled Method, *Metall. Mater. Trans. A—Physical Metallurgy and Materials Science,* Vol 40A (4), 2009, p 943–957.
91. D.G. Eskin, Suyitno, and L. Katgerman, Mechanical Properties in the Semi-Solid State and Hot Tearing of Aluminum Alloys, *Prog. Mat. Sci.,* Vol 49, 2004, p 629–711.

92. A.B. Phillion, S.L. Cockcroft, and P.D. Lee, A Three-Phase Simulation of the Effect of Microstructural Features on Semi-Solid Tensile Deformation, *Acta Mater.,* Vol 56 (16), 2008, p 4328–4338.
93. Y.M. Won and B.G. Thomas, Simple Model of Microsegregation during Solidification of Steels, *Metall. Mater. Trans. A (USA),* Vol 32A (7), 2001, p 1755–1767.
94. T. Matsumiya, H. Kajioka, S. Mizoguchi, Y. Ueshima, and H. Esaka, *Trans. Iron Steel Inst. Jpn.,* Vol 24, 1984, p 873–882.
95. J.H. Weiner and B.A. Boley, Elasto-Plastic Thermal Stresses in a Solidifying Body, *J. Mech. Phys. Solids,* Vol 11, 1963, p 145–154.
96. B.G. Thomas and C. Ojeda, Ideal Taper Prediction for Slab Casting, *ISSTech Steelmaking Conference,* Vol 86, April 27–30, 2003 (Indianapolis, IN), 2003, p 396–308.
97. J. Sengupta and B.G. Thomas, Effect of a Sudden Level Fluctuation on Hook Formation during Continuous Casting of Ultra-Low Carbon Steel Slabs, *Modeling of Casting, Welding, and Advanced Solidification Processes XI (MCWASP XI) Conference*, M. Bellet, C.Z. Gandin, and J.E. Allision, Ed., May 28–June 2, 2006 (Opio, France), 2006, p 727–736.
98. C. Li and B.G. Thomas, Maximum Casting Speed for Continuous Cast Steel Billets Based on Sub-Mold Bulging Computation, *Steelmaking Conf. Proc.,* Vol 85, March 10–13, 2002 (Nashville, TN), ISS, Warrendale, PA, 2002, p 109–130.
99. P. Kozlowski, B.G. Thomas, J. Azzi, and H. Wang, Simple Constitutive Equations for Steel at High Temperature, *Metall. Trans. A,* Vol 23A (3), 1992, p 903–918.
100. P.J. Wray, Plastic Deformation of Delta-Ferritic Iron at Intermediate Strain Rates, *Metall. Trans. A,* Vol 7A, Nov 1976, p 1621–1627.
101. P.J. Wray, Effect of Carbon Content on the Plastic Flow of Plain Carbon Steels at Elevated Temperatures, *Metall. Trans. A,* Vol 13A (1), 1982, p 125–134.
102. T. Suzuki, K.H. Tacke, K. Wunnenberg, and K. Schwerdtfeger, Creep Properties of Steel at Continuous Casting Temperatures, *Ironmaking Steelmaking,* Vol 15 (2), 1988, p 90–100.
103. F. Costes, A. Heinrich, and M. Bellet, 3-D Thermomechanical Simulation of the Secondary Cooling Zone of Steel Continuous Casting, *Proc. MCWASP X, Tenth Int. Conf. on Modeling of Casting, Welding and Advanced Solidification Processes*, D.M. Stefanescu, J.A. Warren, M.R.J. and M.J.M. Krane, Ed., The Minerals, Metals and Materials Society, Warrendale, PA, 2003, p 393–400.
104. D.L. Donsbach and M.W. Moyer, Ultrasonic Measurement of Elastic Constants at Temperatures from 20 to 1100 °C, *Ultrasonic Materials Characterization,* H. Berger and M. Linzer, Ed., June 7–9, 1978 (Gaithersburg, MD), National Bureau of Standards, Special Pub. 596, Nov 1980.
105. O.M. Puhringer, Strand Mechanics for Continuous Slab Casting Plants, *Stahl Eisen,* Vol 96 (6), 1976, p 279–284.
106. D.R. Hub, "Measurement of Velocity and Attenuation of Sound in Iron up to the Melting Point," paper 551, Proc. IVth Int. Vong. Acoustics (Copenhagen), 1962.
107. H. Mizukami, K. Murakami, and Y. Miyashita, Mechanical Properties of Continuously Cast Steels at High Temperatures, *Tetsu-to-Hagane,* Vol 63 (146), 1977, p S 652.
108. C. Li and B.G. Thomas, Thermo-Mechanical Finite Element Model of Bulging and Hot Tearing during Continuous Casting of Steel Billets, *Modeling of Casting, Welding, and Advanced Solidification Processes*, Vol X, D. Stefanescu, J. Warren, M. Jolly, and M. Krane, Ed., May 25–30, 2003 (San Destin, FL), TMS, Warrendale, PA, 2003, p 385–392.
109. K. Harste, A. Jablonka, and K. Schwerdtfeger, Shrinkage and Formation of Mechanical Stresses during Solidification of Round Steel Strands, *Fourth Int. Conf. on Continuous Casting* (Centres de Recherches Metallurgiques and Verein Deutscher Eisenhuttenleute), Stahl und Eisen, Brussels, 1988, p 633–644.
110. K. Harste, "Investigation of the Shrinkage and the Origin of Mechanical Tension during the Solidification and Successive Cooling of Cylindrical Bars of Fe-C Alloys," Ph.D. dissertation thesis, Technical University of Clausthal, 1989.
111. I. Jimbo and A. Cramb, The Density of Liquid Iron-Carbon Alloys, *Metall. Trans. B,* Vol 24B, 1993, p 5–10.
112. E. Howard and D. Lorento, Development of High Speed Casting, *1996 Electric Furnace Conference Proceedings,* Dec 9–12, 1996 (Dallas, TX), ISS, Warrendale, PA, 1996.